npj | 2D materials and applications

Article

Published in partnership with FCT NOVA with the support of E-MRS

https://doi.org/10.1038/s41699-024-00460-1

# Hard ferromagnetism in van der Waals $Fe_3GaTe_2$ nanoflake down to monolayer

Check for updates

Mingjie Wang[1], Bin Lei[1], Kejia Zhu[1], Yazhou Deng[1], Mingliang Tian[1], Ziji Xiang[2], Tao Wu[2] & Xianhui Chen[2,3,4]

Two-dimensional (2D) magnetic materials are of not only fundamental scientific interest but also promising candidates for numerous applications. However, so far only a few intrinsic magnets with long-ranged order down to the 2D limit have been experimentally established. Here, we report that the intrinsic 2D ferromagnetism can be realized in van der Waals (vdW) $Fe_3GaTe_2$ nanoflake down to monolayer. By measuring the Hall resistance and magnetoresistance, we demonstrate that the $Fe_3GaTe_2$ monolayer exhibits 2D hard ferromagnetism with record-high Cure temperature ($T_c$) of 240 K for the monolayer of known intrinsic ferromagnets. Both of square-shaped hysteresis loops with near-vertical jump in anomalous Hall effect (AHE) and the negative magnetoresistance (NMR) behavior with an applied out-of-plane magnetic field reveal robust perpendicular magnetic anisotropy (PMA) in $Fe_3GaTe_2$ nanoflakes down to the monolayer limit. Furthermore, we find the intrinsic mechanism that stems from the Berry curvature of electronic bands dominates AHE of nanoflakes in the low temperature range. Our results not only provide an excellent candidate material for next-generation spintronic applications, but also open up a platform for exploring physical mechanisms in 2D ferromagnetism.

In the past decades, research on two-dimensional (2D) materials has attracted great research interest due to their physical properties and potential applications[1–10]. In particular, the recent discovery of 2D magnetic materials, which present intrinsic ferromagnetic/antiferromagnetic ground states at finite temperatures down to atomic-layer thicknesses, offers possibilities for both fundamental research and the potential applications of spintronic devices[8–11]. Layered van der Waals bulk magnetic materials facilitate their atomic-layer cleavability and magnetic anisotropy, providing an ideal platform for theoretically and experimentally exploring quantum phenomena in the 2D limit. Unfortunately, finding suitable vdW materials and producing atomically thin magnetic materials have been a challenge. Up to now, there have been only a few reports of producing atomically thin samples of magnetic materials and the observation of magnetic ordering in the 2D limit, such as $FePS_3$[8], $CrI_3$[9], and so on. However, the magnetic transition temperature of these 2D materials is much lower than room temperature, which limits their practical application. Hence, it is necessary to explore more 2D magnetic materials to achieve higher magnetic transition temperatures.

Among layered vdW magnetic materials, $Fe_NGeTe_2$ ($N = 3, 4, 5$) family is particularly remarkable due to its high Curie temperature and vast tunability of magnetic properties[11–20]. 2D ferromagnetism has been observed in $Fe_3GeTe_2$ and $Fe_5GeTe_2$ nanoflakes[11,12,20]. Recently, a vdW intrinsic ferromagnetic crystal $Fe_3GaTe_2$, which has the same structure as $Fe_3GeTe_2$, was reported to exhibit record-high Curie temperature (350–380 K) for known layered vdW intrinsic ferromagnets[21]. The robust large perpendicular magnetic anisotropy (PMA) and high Curie temperature are beneficial for experimentally exploring magnetic properties down to the 2D limit. Above-room-temperature Curie temperature has been observed in $Fe_3GaTe_2$ nanoflakes with the thickness of 9.5 nm[21]. Therefore, it is highly anticipated whether its monolayer sample can maintain ferromagnetism and achieve above-room-temperature Curie temperature.

In this work, we have successfully prepared $Fe_3GaTe_2$ nanoflakes with thickness ranging from bulk to monolayer. As corroborated by Hall resistance and magnetoresistance measurements, all samples present hard ferromagnetism at low temperature. Strikingly, the $Fe_3GaTe_2$ monolayer exhibits 2D hard ferromagnetism with record-high Curie temperature ($T_c$)

[1]School of Physics and Optoelectronic Engineering, Anhui University, Hefei, Anhui 230601, China. [2]CAS Key Laboratory of Strongly-coupled Quantum Matter Physics, Department of Physics, University of Science and Technology of China, Hefei, Anhui 230026, China. [3]CAS Center for Excellence in Quantum Information and Quantum Physics, Hefei, Anhui 230026, China. [4]Collaborative Innovation Center of Advanced Microstructures, Nanjing University, Nanjing, Jiangsu 210093, China. e-mail: leibin@ahu.edu.cn; chenxh@ustc.edu.cn

of 240 K for known intrinsic vdW ferromagnetic single layer. Square-shaped hysteresis loops with near-vertical jump in AHE and the NMR behavior with an applied out-of-plane magnetic field have been observed, suggesting robust PMA in $Fe_3GaTe_2$ nanoflakes. Our results compensate for the unexplored electronic and magnetic properties of $Fe_3GaTe_2$ down to the 2D limit and open up opportunities for next-generation spintronic applications.

## Results

### Magnetic properties of $Fe_3GaTe_2$ single crystal

$Fe_3GaTe_2$ crystallizes in a hexagonal structure (space group $P6_3/mmc$), which consists of layered building blocks stacking along the *c*-axis[21]. As shown in Fig. 1a, each of these blocks contains two layers of Te atoms and a Fe-Ga slab with two different Fe atom sites (Fe1 and Fe2) sandwiched between the two Te layers. The van der Waals (vdW) gap between two adjacent blocks makes crystals cleavable. In this work, we define one such block as one vdW layer (a monolayer, 1 L, with a thickness of ~ 0.8 nm) for $Fe_3GaTe_2$; thus, one unit cell is composed of two layers (2 L). The plate-like $Fe_3GaTe_2$ single crystals with the typical size of $2 \times 2 \times 0.1$ $mm^3$ were grown via a self-flux method. A detailed growth procedure is described in the methods section. The X-ray diffraction (XRD) of as-grown $Fe_3GaTe_2$ bulk crystals is displayed in Supplementary Fig. 1. Only (00 *l*) peaks are observed, implying the strict orientation growth and high crystallinity. The calculated *c*-axis lattice parameter is 16.19 Å, consistent with previous reported results[21]. The chemical compositions of these crystals were identified by the energy dispersive spectroscopy (EDS), revealing the averaged atomic ratio as Fe : Ga : Te = 3.05 : 0.97 : 2 (Supplementary Table 1), in good agreement with the stoichiometric ratio.

Figure 1b displays the temperature-dependent magnetization (*M*–*T*) measurements performed with zero-field-cooling (ZFC) and field-cooling (FC) conditions under an applied magnetic field of 0.1 T. The single crystals show a typical ferromagnetic feature and the Curie temperature ($T_c$) estimated by the maximum of $|dM/dT|$ is about 340 K (Supplementary Fig. 1b), which is consistent with recent reports[22]. Over the entire temperature range from 2 to 300 K, the magnetization for *H* // *c* is much larger than that of *H* // *ab*, indicating a perpendicular magnetic anisotropy (the *c*-axis is the easy-magnetization axis). A clear split is observed on the ZFC and FC curves at low temperature, which is a characteristic behavior of ferromagnets and implies the formation of a multi-domain magnetic structure[23]. Figure 1c shows the isothermal *M*–*H* curves measured for $Fe_3GaTe_2$ single crystals at the temperature range from 2 to 400 K between -5 T and 5 T. Solid and dashed lines are data for *H* // *c* and *H* // *ab*, respectively. Typical magnetic hysteresis loops are observed when the magnetic field is along the out-of-plane orientation (*H* // *c*), while vanish under the in-plane orientation (*H* // *ab*), further suggesting the out-of-plane magnetic anisotropy in bulk $Fe_3GaTe_2$. It should be noted that *M*–*H* curves for *H* // *c* exhibits a relatively large coercivity field ($H_c$ ~ 110 mT) at 2 K, implying hard ferromagnetism in bulk samples. In addition, the saturation magnetization ($M_s$) of $Fe_3GaTe_2$ bulk crystal decreases with increasing temperature, but it drops slowly below 150 K (Supplementary Fig. 1c).

### Characterization of $Fe_3GaTe_2$ nanoflakes

To investigate the thickness-dependent magnetic properties, we fabricated devices with Hall bar configurations based on atomically thin $Fe_3GaTe_2$ thin flakes. Since it is difficult to obtain ultrathin flakes using the conventional scotch tape method, we utilized the previously reported $Al_2O_3$-assisted exfoliation technique[11,24,25] and successfully obtained sizable thin flakes with thickness approaching to the 2D limit. A detailed device preparation procedure is described in the methods section. Figure 2a and Supplementary Fig. 2a, c show the optical transmission image of few-layer $Fe_3GaTe_2$ flakes exfoliated by an $Al_2O_3$ film on top. The whole stack is attached to a piece of transparent polydimethylsiloxane (PDMS) film. Regions with different layer numbers (1 L, monolayer; 2 L, bilayer; 3 L, trilayer; 4 L, four-layer; 5 L, five-layer; 6 L, six-layer) are marked out. In this work, the thickness of ultra-thin $Fe_3GaTe_2$ nanoflakes can be determined by combination of atomic force microscopy (AFM) and optical transmission measurements (Supplementary Fig. 2), and thick flakes are identified just by AFM measurements (Supplementary Fig. 3b). The optical transmission is defined as $T = G^T_{sample}/G^T_{substrate}$, where $G^T_{sample}$ and $G^T_{substrate}$ are the transmission intensities of the sample ($Fe_3GaTe_2$ nanoflakes) and the substrate (PDMS and $Al_2O_3$ films). As shown in Fig. 2b, the relationship between the optical transmission and the flake thickness for three different samples all follow the Beer-Lambert law: log(T) = 1 - $K$ × (layer number), where $K$ is the absorption coefficient[11]. Therefore, the layer number can be determined precisely by the optical transmission. Moreover, the layer identification was also corroborated by atomic force

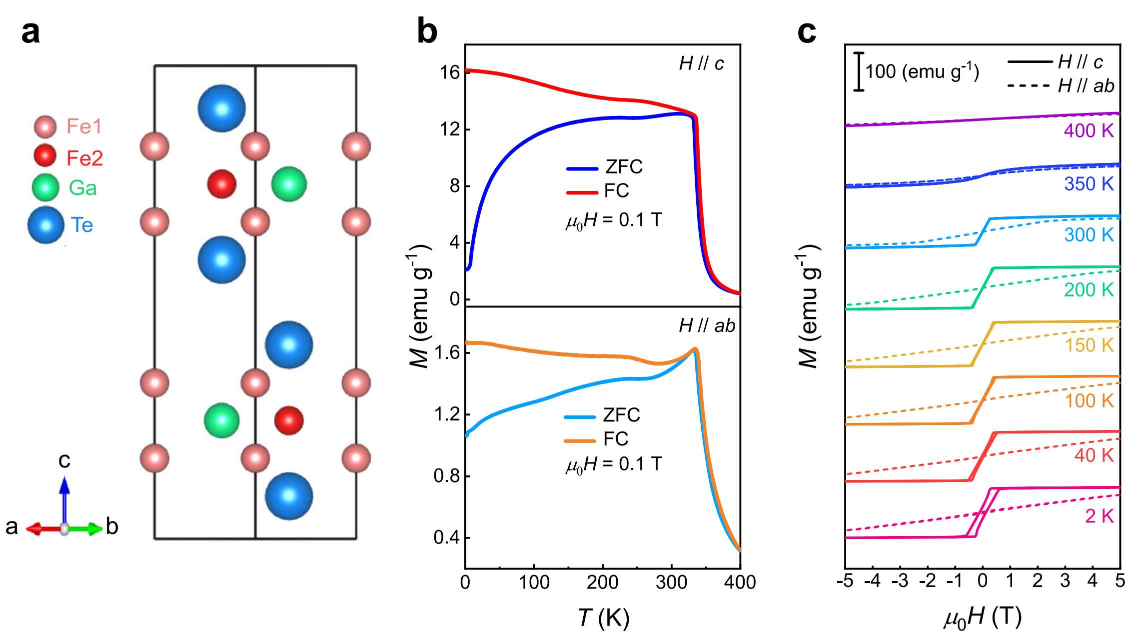


**Fig. 1 | Crystal structure and magnetic properties of $Fe_3GaTe_2$ single crystal.** **a** Schematic diagram of the crystal structure of $Fe_3GaTe_2$. **b** Temperature-dependent magnetization of $Fe_3GaTe_2$ single crystal measured with $\mu_0H$ = 0.1 T applied within *ab*-plane and along *c*-axis in both ZFC and FC modes. **c** *M*–*H* curves measured at various temperatures between −5 and 5 T for $Fe_3GaTe_2$ bulk crystal. Solid and dashed lines are data for *H* // *c* and *H* // *ab*, respectively.

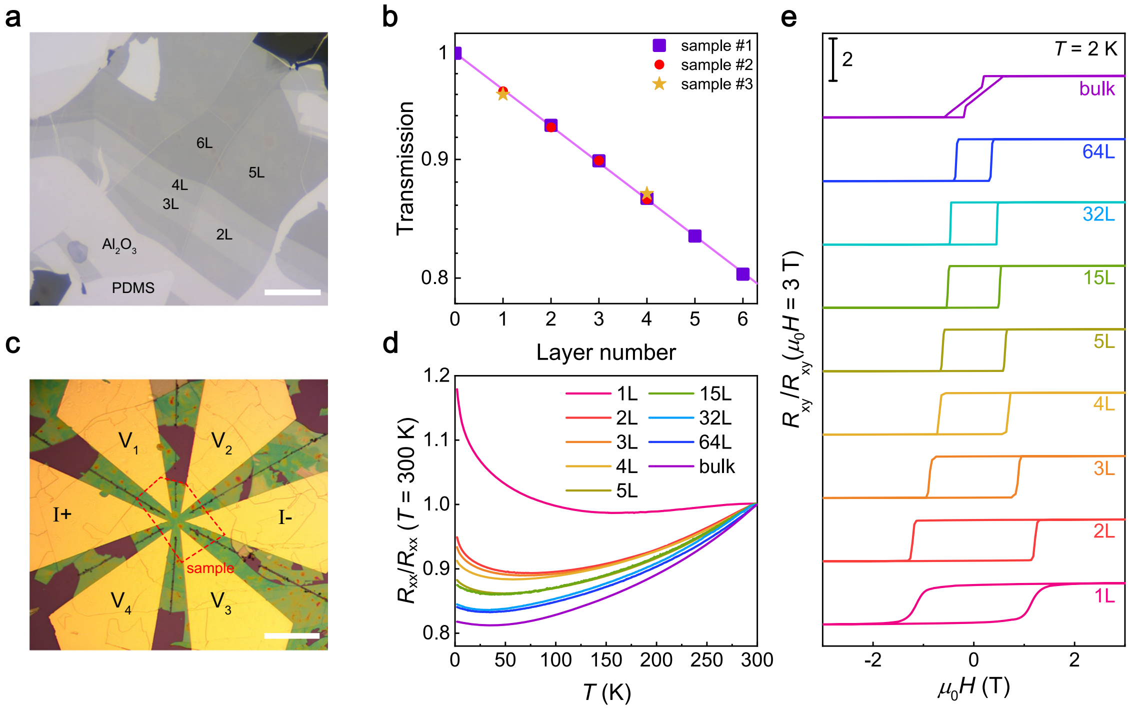


**Fig. 2 | Characterization of $Fe_3GaTe_2$ nanoflakes. a** A typical optical transmission image of few-layer $Fe_3GaTe_2$ flakes exfoliated on top of $Al_2O_3$ film supported on a piece of transparent polydimethylsiloxane (PDMS) substrate. Regions with different layer numbers (2L-6L) are marked out. Scale bar: 50um. **b** Optical transmission as a function of the layer number. The values of transmission marked by purple squares are extracted from Fig. 2a (sample #1), the red dots are extracted from sample #2 (Supplementary Fig. 2a), and the yellow stars are extracted from sample #3 (Supplementary Fig. 2c) whose thickness has been checked by atomic force microscopy measurements (Supplementary Fig. 2e, f). Both of them follow the Beer-Lambert law (mauve straight line). **c** A representative optical image of the device with the $Fe_3GaTe_2$ nanoflake. I+ and I- label the current electrodes, and $V_1$, $V_2$, $V_3$ and $V_4$ label the voltage probes. Scale bar: 50um. **d** The evolution of the temperature-dependent longitudinal resistance $R_{xx}$ for $Fe_3GaTe_2$ flakes with different thicknesses. Resistances are normalized by their values at $T = 300$K. **e** Normalized Hall resistance $R_{xy}(H)$ curves at 2 K for samples with different thicknesses.

microscope (AFM) measurements. The 0.8 nm and 3.2 nm steps in the height profiles exactly match the 1 L and 4 L thicknesses for $Fe_3GaTe_2$ flakes (Supplementary Fig. 2e, f). An optical image of the typical device based on $Fe_3GaTe_2$ flake is illustrated in Fig. 2c. The six-probe configuration facilitates us to simultaneously measure the longitudinal resistance ($R_{xx}$) and Hall resistance ($R_{xy}$). Figure 2d shows the temperature-dependent normalized longitudinal resistance $[R_{xx}/R_{xx}(300\mathrm{K})]$ for the $Fe_3GaTe_2$ samples with thicknesses varying from bulk to monolayer. The bulk crystal exhibits a typical metal behavior. As the thickness decreases, the longitudinal resistance ($R_{xx}$) of the thin flake gradually increases rapidly at low temperature. Unlike other samples, the monolayer sample exhibits semiconductor-like behavior, which may be caused by the electron localization and interaction effects in 2D disordered system[26–28] (see Supplementary Note 1). It should be pointed out that the upturn of low-temperature resistance in monolayer and bilayer flakes can be well depicted by the 2D Mott variable-range-hopping (VRH) model yielding $\ln(R_{xx}) \sim T^{-1/3}$ (see Fig. 4b). Similar behaviors have been reported in other vdW ferromagnetic thin flakes, such as $Fe_3GeTe_2$[29,30] and $Fe_5GeTe_2$[20].

### Anomalous Hall effect in $Fe_3GaTe_2$

As shown above, $Fe_3GaTe_2$ bulk crystal exhibits hard ferromagnetism. It is generally believed that in ferromagnets, the total Hall resistance $R_{xy}$ can be expressed as $R_{xy} = R^0_{xy} + R^A_{xy} = R_0\mu_0H + R_sM$, where $R^0_{xy}$ and $R^A_{xy}$ are the normal and anomalous Hall resistance respectively, and $R_0$ and $R_s$ are the ordinary and anomalous Hall coefficients, respectively[31,32]. Since $R^A_{xy}$ scales with magnetization ($M$), it is suitable to study the evolution of magnetism with thickness in $Fe_3GaTe_2$ nanoflakes by measuring the anomalous Hall resistance. Figure 3 presents the temperature-dependent Hall resistance $R_{xy}$ for $Fe_3GaTe_2$ with various thicknesses. The $R_{xy}(H)$ curves at low temperature for all exfoliated thin flakes exhibit sizable square-shaped hysteresis loops with near-vertical jump, which is the hallmark of hard ferromagnetism with single-domain structure. However, the bulk crystal displays a step-like hysteresis loop. When the applied magnetic field sweeps from the positive saturation field to the negative saturation field, the $R_{xy}$ value first drops sharply and then decreases slowly. This behavior generally tracks the $M$–$H$ curves, suggesting a multi-domain structure. Such a large difference of $R_{xy}(H)$ curves between thin flakes and bulk crystal may be attributed to the thickness-dependent magnetic domain transformation[12,15]. Similar result has been observed in previously reported $Fe_3GaTe_2$ nanosheets with different thicknesses[21].

In particular, we selected the $R_{xy}(H)$ curves at 2 K and normalized them to explore the evolution of the coercivity field ($H_c$) with thickness, as shown in Fig. 2e. Inspiringly, a sizable hysteresis loop centered at $H = 0$ with remarkable remanence can be observed in monolayer sample, suggesting intrinsic 2D ferromagnetism in the $Fe_3GaTe_2$ monolayer. Such observation is complemented by the magnetoresistance (MR) measurements (Supplementary Fig. 5). At low temperature, a bow-tie shaped hysteresis loop has been observed in all samples with various thicknesses, suggesting distinct ferromagnetism even down to the 2D limit. In addition, since the increase of magnetic field applied along the easy axis can reduce the electron-spin scattering[20,33], the negative magnetoresistance (NMR) behavior with applied out-of-plane magnetic field also implies robust PMA in $Fe_3GaTe_2$ nanoflakes. In order to further validate this issue, we performed angular-dependent Hall resistance ($R_{xy}$) measurements at 20 K for $Fe_3GaTe_2$ monolayer sample. As shown in Supplementary Fig. 6, with the decrease of $\theta_H$ from 90° ($H$ // $c$) to 0° ($H$ // $ab$), the $R_{xy}$ changes from an uptrend to a downtrend in the high filed regime ($\mu_0H > 1.5$ T), and the coercive field ($H_c$)

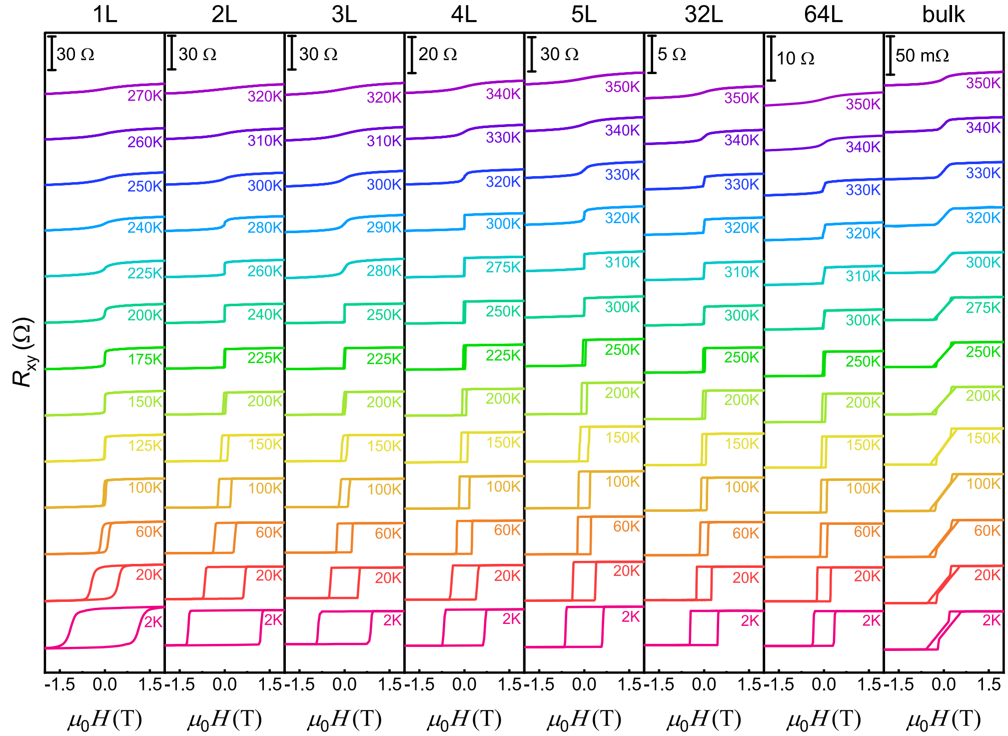


**Fig. 3 | Anomalous Hall effect in $Fe_3GaTe_2$.** Hall resistance $R_{xy}$ at various temperatures measured for $Fe_3GaTe_2$ thin flakes with different thicknesses (1L-64L) and bulk crystal. External magnetic field $H$ is applied along $c$-axis. The scale bars denote the amplitude of Hall resistance for each device.

increases simultaneously. Such behavior is characteristic of ferromagnets with PMA[11,21,29]. In addition, we also extracted the $R_{xy}$ value at $\mu_0H = 3$ T to calculate $\theta_M$ (the angle between magnetization and the basal plane) by using the formula[11]: $\theta_M(\theta_H) = \arcsin\left[\frac{R_{xy}(\theta_H)}{R_{xy}(\theta_H=90^\circ)}\right]$. The calculation result is $\theta_M(\theta_H = 30^\circ) \approx 56^\circ$, and $\theta_M > \theta_H$ also indicates a strong out-of-plane magnetic anisotropy in the monolayer $Fe_3GeTe_2$. The size of hysteresis in $R_{xy}(H)$ curves shows systematical dependence on thickness. The evolution of $H_c$ with thickness in $Fe_3GaTe_2$ nanoflakes at 2 K is summarized in Supplementary Fig. 1d, revealing a very pronounced layer dependence of the coercivity field from 78 mT (bulk) to 1.2 T (2 L) at 2 K. For samples with thickness exceeding two layers, the coercivity field decreases monotonically with the increasing layer number, which is consistent with previous report[21]. Nevertheless, the coercivity field of monolayer sample shows a slight decrease compared to bilayer sample. Meanwhile, the square-shape jump of Hall resistance in the monolayer sample is not as sharp as that for other thicknesses, which may be attributed to the disorder in 2D limit.

### Thickness-dependent ferromagnetism in $Fe_3GaTe_2$

In order to investigate the effect of thermal fluctuations on ferromagnetism, we look into the thickness dependence of the Curie temperature $T_c$. In general, the $T_c$ value can be calibrated by examining the remanent Hall resistance at zero external magnetic field, $R^r_{xy} = R_{xy}(\mu_0H = 0)$, which is proportional to the zero-field spontaneous magnetization $M(\mu_0H = 0)$. In this way, $T_c$ is defined as the temperature at the onset of non-zero $R^r_{xy}$ (Supplementary Note 2). Supplementary Fig. 7c shows thickness-temperature phase diagram based on analysis of $R^r_{xy}$, exhibiting a bizarre dome-like behavior. This result is similar to previously reported $Fe_3GeTe_2$[12], which can be understood as a temperature-driven magnetic domain formation in thick samples. That is to say, the $T_c$ value determined by the onset of non-zero $R^r_{xy}$ contains the influence of the magnetic domain wall formations. Hence, in this work we tend to define the $T_c$ of $Fe_3GaTe_2$ thin flakes based on analysis of the Arrott plot of the AHE (see Supplementary Note 3 and Supplementary Fig. 8). The $T_c$ value is determined by extrapolating high-field data where domains are fully aligned, which minimizes the effects of domain wall formation[34]. Arrott plots analysis reveal that $T_c$ decreases monotonically as the samples are thinned down from 5 L to 1 L, whilst it barely changes for thickness above 15 L, as shown in Fig. 4a. This large drop in $T_c$ near the 2D limit roughly follows a universal scaling law of ultrathin magnetic films[35]. Surprisingly, the monolayer still maintains a relatively high $T_c$ (~240 K), record-high for known intrinsic vdW ferromagnetic monolayer[9,11,12,20].

### Scaling analysis of the anomalous Hall effect

In addition, we also analyze the dominant mechanism of AHE in $Fe_3GaTe_2$ ultra-thin flakes. It is generally accepted that there are three main mechanisms which contribute to AHE: one is intrinsic AHE that stems from the Berry curvature of electronic bands, the other two are extrinsic mechanisms, named as skew scattering and side jump, respectively[31]. Here, we use the scaling model[36] as followed to describe the AHE:

$$R^A_{xy}(T) = \left(\alpha R_{xx0} + \beta R^2_{xx0}\right) + bR^2_{xx}(T) \tag{1}$$

Since the resistivity of our thin flake is difficult to calculate precisely, we perform a scaling analysis based on the resistance values. In this model, $R_{xx0}$ is the residual resistance, $R_{xx}$ denotes the longitudinal resistance, the coefficients $\alpha$, $\beta$ indicate the amplitudes of the AHE terms contributed by two extrinsic mechanisms, skew scattering and side jump, whereas, $b$ determine the intrinsic mechanism. In our measurements, $R^A_{xy} \gg R^0_{xy}$, $R_{xx} \gg R_{xy}$, thus, the anomalous Hall conductance (AHC) $G^A_{xy}$ and the longitudinal conductance $G_{xx}$ can be expressed as

$$G^A_{xy} = \frac{R^A_{xy}}{\left(R^A_{xy}\right)^2 + \left(R_{xx}\right)^2} \tag{2}$$

$$G_{xx} = \frac{R_{xx}}{\left(R^A_{xy}\right)^2 + \left(R_{xx}\right)^2} \approx \frac{1}{R_{xx}} \tag{3}$$

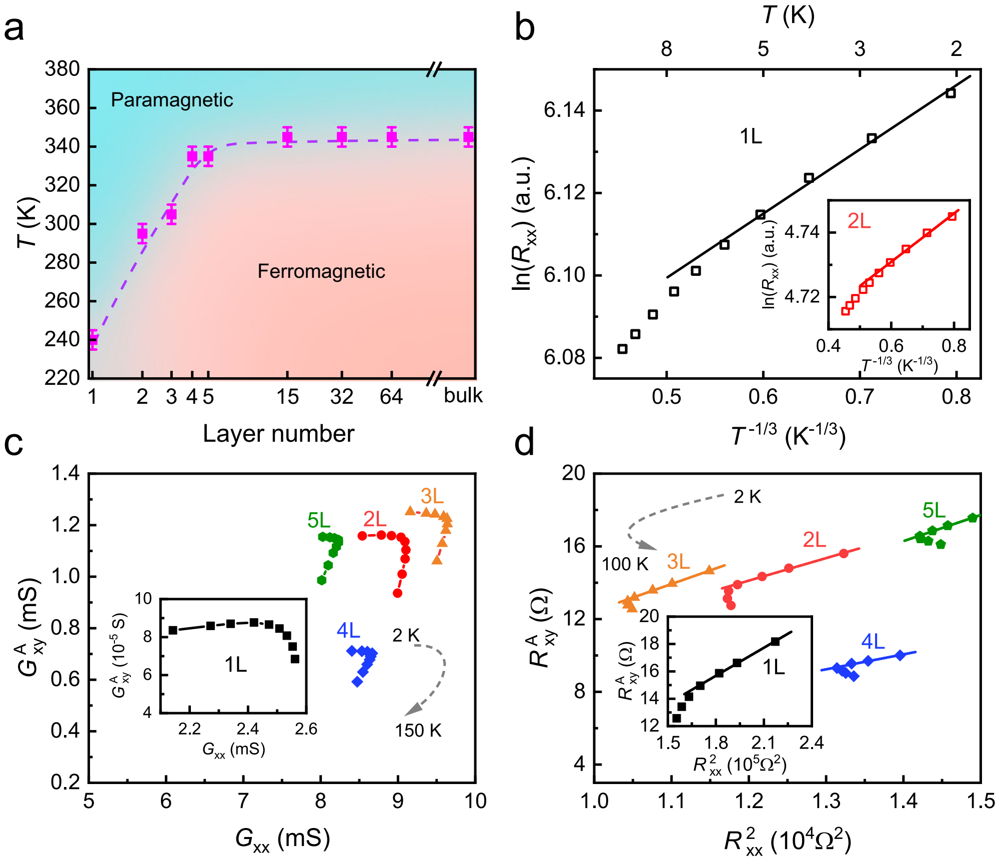


**Fig. 4 | Thickness-dependent ferromagnetism in $Fe_3GaTe_2$. a** Phase diagram of $Fe_3GaTe_2$ thin flakes showing the dimensionality effect of the magnetism. The Curie temperature $T_c$ is determined for each layer number by analysis of the Arrott plot of the AHE (Supplementary Fig. 8). The error bars represent uncertainties in defining the onset temperature of non-zero $R^s_{xy}$. The bottom of the error bar represents the temperature that $R^s_{xy}$ starts to be greater than zero, while the top of the error bar represents the temperature that $R^s_{xy}$ begins to be less than zero. **b** $\ln(R_{xx})$ measured in the monolayer and bilayer (the inset) $Fe_3GaTe_2$ devices as functions of $T^{-1/3}$. Straight lines denote fits using the 2D Mott variable-range-hopping model: $\ln(R_{xx}) \sim T^{-1/3}$. **c** Anomalous Hall conductance $G^A_{xy}$ plotted against the longitudinal conductance $G_{xx}$ for $Fe_3GaTe_2$ thin flakes with thicknesses between 2 L and 5 L. Inset displays the monolayer case. Along the direction of the grey dotted line, the temperatures from low to high in turn are 2, 10, 20, 40, 60, 80, 100, 125, 150 K. **d** Anomalous Hall resistance $R^A_{xx}$ as a function of $R^2_{xx}$ in few layer samples (2L-5L). The inset showcases $R^A_{xx}$ vs $R^2_{xx}$ for the monolayer device. Apparent linear behavior can be seen in the low-temperature region. Along the direction of the grey dotted line, the temperatures from low to high in turn are 2, 10, 20, 40, 60, 80, 100 K. Almost all kinks in (c) and (d) are about 60 K.

Equation 1 can also be written in the form of conductance consequently:

$$G^A_{xy}(T) = \left(\alpha {G_{xx0}}^{-1} + \beta {G_{xx0}}^{-2}\right) G^2_{xx}(T) + b \tag{4}$$

We note that the saturation magnetization ($M_s$) of bulk sample decreases slowly below 150 K, but falls drastically above 150 K (Supplementary Fig. 1c). In order to reduce the interference of the varying $M_s$ on the scale analysis, we just extract the values of $R_{xx}$ and $R_{xy}$ below 150 K in our nanoflakes for scaling analysis, assuming that $M_s$ is essentially constant in this temperature range. In Supplementary Fig. 9, we show the temperature-dependent normalized anomalous Hall resistance $R^A_{xy}$ and anomalous Hall conductance $G^A_{xy}$ for $Fe_3GaTe_2$ thin flakes with thicknesses from 1 L to 5 L. When the temperature is below 60 K, the $G^A_{xy}$ of 1 L to 5 L flakes is almost independent of the temperature. We focus on the scaling model Eq. 4, the $G^A_{xy}$ versus $G_{xx}$ plot is shown in Fig. 4c. It is noticeable that there is a constant part for $G^A_{xy}$ which is independent of $G_{xx}$ and temperature below 60 K for all nanoflakes with thicknesses from 1 L to 5 L, which points towards the dominance of the intrinsic AHE. Similar results have been observed in $Fe_3GaTe_2$ nanosheets with thicknesses of 27.2 nm and 10 nm below 100 K in a recent study[37]. These results all indicate that the AHE in $Fe_3GaTe_2$ at low temperature arises from an intrinsic mechanism. Furthermore, in the $R^A_{xy}$ versus $R^2_{xx}$ plot (Fig. 4d), the apparent linear behavior of the low-temperature region also confirms the contribution of the intrinsic AHE[38], according to Eq. 1. In particular, we find a significant decrease in the slope of the low-temperature linear part in monolayer compared to the other layers. The intrinsic AHE dramatically decreases as the thickness reaches the 2D limit, indicating that the size effect may change the Berry curvature contribution[39]. Almost all kinks in the $G^A_{xy} - G_{xx}$ and $R^A_{xy} - R^2_{xx}$ curves are around 60 K. Above 60 K, $G^A_{xy}$ versus $G_{xx}$ appears to be linear and the intrinsic mechanism does not dominate the AHE. The emergence of these kinks seems to be related to the nonmonotonic $R_{xx}(T)$ and similar results have been observed in the high pressure-modulated $Fe_3GeTe_2$[40]. Our results just reveal that the intrinsic mechanism dominates the AHE of 2D $Fe_3GaTe_2$ at low temperature and further investigations are required to clarify the mechanism.

## Discussion

In summary, we systematically investigated the layer-number dependent magnetic properties in $Fe_3GaTe_2$ down to 2D limit by analyses of MR and AHE. Strikingly, the $Fe_3GaTe_2$ monolayer exhibits a true 2D hard ferromagnetism with a record-high $T_c$ of 240 K for known intrinsic vdW ferromagnetic single layer. Square-shaped hysteresis loops in AHE and the NMR behavior with a magnetic field applied along *c*-axis have been observed in atomically thin flakes, indicting robust PMA in $Fe_3GaTe_2$ nanoflakes down to the monolayer limit. Besides, we find the intrinsic mechanism that stems from the Berry curvature of electronic bands dominates AHE of nanoflakes in low-temperature range based on the scaling analysis in ultra-thin films. Our results compensate for the undiscovered electronic and magnetic properties of $Fe_3GaTe_2$ in the 2D limit, providing a reference for practical applications of next-generation spintronic devices and opening up a platform for exploring physical mechanisms in high-temperature 2D ferromagnetism.

## Methods

### Crystal growth and characterizations

High-quality bulk $Fe_3GaTe_2$ single crystals were grown via a self-flux method[21]. High-purity Fe powders (Aladdin, 99.95%), Ga lumps (Aladdin, 99.999%), and Te powders (Aladdin, 99.999%) were mixed in the molar ratio of Fe : Ga : Te = 3 : 1 : 2 in an argon-filled glove box and loaded into a quartz tubes. The sealed quartz tubes were placed into a muffle furnace. It was first heated to 1000°C and held for 3 days for solid reactions. Then the temperature was quickly decreased down to 900°C and slowly cooled down to 800°C in 5 days, followed by slowly cooled down to room temperature. The shiny plate-shaped $Fe_3GaTe_2$ single crystals with a typical size of 2 mm×2 mm×0.1 mm were selected from the ingot (Supplementary Fig. 1a inset). The crystallographic phase of these single crystals was characterized using room-temperature X-ray diffraction (XRD) measurements (SmartLab-9, Rigaku Corp.) with Cu Kα radiation (λ = 1.5406 Å) (Supplementary Fig. 1a), and the actual chemical compositions were identified by the energy dispersive spectroscopy (EDS) at different microregions on the fresh cleavage surfaces of the same single crystal. Supplementary Table 1 shows the mole ratio of 5 random microregions on one of these samples, and the averaged mole ratio was revealed as Fe: Ga: Te = 3.05: 0.97: 2, which almost consisted with the stoichiometric ratio.

### Devices fabrication

The $Fe_3GaTe_2$ thin flakes with thickness above 12 nm (≈15 L) were mechanically exfoliated from the plate-like bulk single crystals using the scotch tape and the polydimethylsiloxane (PDMS) film, and were transferred onto the surface of 300 nm thick $SiO_2$ insulating layer grown on a highly doped Si substrate. However, ultrathin flakes of $Fe_3GaTe_2$ (1–5 L) were obtained by the previously developed $Al_2O_3$-assisted exfoliation technique[11,20]. In this process, we first deposited an $Al_2O_3$ thin film onto the prepared fresh cleavage surface of the bulk crystal, then used a thermal release tape to peal the $Al_2O_3$ film with $Fe_3GaTe_2$ flakes attached. Scotch tapes were then utilized to exfoliate the $Fe_3GaTe_2/Al_2O_3$ stack repeatedly until $Fe_3GaTe_2$ thin flakes with suitable size and thickness appeared. After that, the $Fe_3GaTe_2/Al_2O_3$ stack was released onto a piece of PDMS film by heating the tape. Since the PDMS and $Al_2O_3$ films are almost transparent, we can use the transmission mode of the optical microscope to determine the sample thickness before transferring the flakes onto a $SiO_2$/Si substrate. In this work, the layer number of $Fe_3GaTe_2$ below 5 was calibrated by the combination of atomic force microscopy (AFM) and the Beer-Lambert law describing the relationship between optical transmission and thickness, whereas the layer number above 15 was determined just via atomic force microscope (AFM) thanks to the low recognition of the Beer-Lambert law in high thickness intervals. Supplementary Fig. 3b shows an AFM scan image of one microregion in the optical picture (Supplementary Fig. 3a), which indicates the thickness of this flake is approximately 12 nm (≈15 L). After transferring the $Fe_3GaTe_2/Al_2O_3$ stack from a PDMS film onto the substrate, Cr/Au (10/120 nm) electrodes were deposited on flakes using stencil masks for transport measurements. It's worth noting that the flakes with different thicknesses are always adjacent to each other on the same substrate. To guarantee that the measured flakes are of uniform thickness, we used a needle tip to cut the current channel connecting flakes of different thicknesses. However, this process results in $Fe_3GaTe_2$ nanoflakes not being an ideal Hall bar configuration, therefore, we cannot accurately calculate the resistivity and Hall resistivity of the samples. In order to preserve the flakes from degradation, the whole process of device preparation was operated in the glovebox with Ar atmosphere ($H_2O$ < 0.1 ppm, $O_2$ < 0.1 ppm). Before taking the device out of the glove box, we first installed the device into a customer-designed puck (Supplementary Fig. 2b), which was sealed with vacuum grease in the glove box. Furthermore, the whole package was then immediately loaded into a commercial physical property measurement system (PPMS DynaCool, Quantum Design) within 1 min.

### Experimental measurements

The magnetic properties of $Fe_3GaTe_2$ bulk crystals were characterized by the SQUID system (Quantum Design) equipped with a vibrating sample magnetometer (VSM) in both out-of-plane ($H$ // $c$) and in-plane ($H$ // $ab$) directions, and the electric transport properties were measured by a physical property measurement system (PPMS DynaCool, Quantum Design). In the measurements of hysteresis loop in MR and AHE in $Fe_3GaTe_2$ thin flakes, we first raised the magnetic field to +3 T (the value greater than the saturation magnetic field of $Fe_3GaTe_2$, direction along out-of-plane), then took the curve with the field continuously swept to -3T and back to +3 T.

## Data availability

All data supporting the findings of this study are included in the paper and its Supplementary Information files. The corresponding author can also provide additional data upon reasonable request.

Received: 30 October 2023; Accepted: 7 March 2024;
Published online: 18 March 2024

## References

1. Novoselov, K. S. et al. Electric Field Effect in Atomically Thin Carbon Films. *Science* **306**, 666–669 (2004).
2. Yu, Y. et al. High-temperature superconductivity in monolayer $Bi_2Sr_2CaCu_2O_{8+\delta}$. *Nature* **575**, 156–163 (2019).
3. Radisavljevic, B., Radenovic, A., Brivio, J., Giacometti, V. & Kis, A. Single-layer $MoS_2$ transistors. *Nat. Nanotechnol.* **6**, 147–150 (2011).
4. Li, L. et al. Black phosphorus field-effect transistors. *Nat. Nanotechnol.* **9**, 372–377 (2014).
5. Fei, Z. et al. Ferroelectric switching of a two-dimensional metal. *Nature* **560**, 336–339 (2018).
6. Lu, J. M. et al. Evidence for two-dimensional Ising superconductivity in gated $MoS_2$. *Science* **350**, 1353–1357 (2015).
7. Saito, Y., Kasahara, Y., Ye, J., Iwasa, Y. & Nojima, T. Metallic ground state in an ion-gated two-dimensional superconductor. *Science* **350**, 409–413 (2015).
8. Lee, J.-U. et al. Ising-Type Magnetic Ordering in Atomically Thin $FePS_3$. *Nano Lett.* **16**, 7433–7438 (2016).
9. Huang, B. et al. Layer-dependent ferromagnetism in a van der Waals crystal down to the monolayer limit. *Nature* **546**, 270–273 (2017).
10. Gong, C. et al. Discovery of intrinsic ferromagnetism in two-dimensional van der Waals crystals. *Nature* **546**, 265–269 (2017).
11. Deng, Y. et al. Gate-tunable room-temperature ferromagnetism in two-dimensional $Fe_3GeTe_2$. *Nature* **563**, 94–99 (2018).
12. Fei, Z. et al. Two-dimensional itinerant ferromagnetism in atomically thin $Fe_3GeTe_2$. *Nat. Mater.* **17**, 778–782 (2018).
13. Kim, K. et al. Large anomalous Hall current induced by topological nodal lines in a ferromagnetic van der Waals semimetal. *Nat. Mater.* **17**, 794–799 (2018).
14. Zhang, Y. et al. Emergence of Kondo lattice behavior in a van der Waals itinerant ferromagnet, $Fe_3GeTe_2$. *Sci. Adv.* **4**, eaao6791 (2018).
15. Tan, C. et al. Hard magnetic properties in nanoflake van der Waals $Fe_3GeTe_2$. *Nat. Commun.* **9**, 1554 (2018).
16. Seo, J. et al. Nearly room temperature ferromagnetism in a magnetic metal-rich van der Waals metal. *Sci. Adv.* **6**, eaay8912 (2020).
17. May, A. F. et al. Ferromagnetism Near Room Temperature in the Cleavable van der Waals Crystal $Fe_5GeTe_2$. *ACS Nano* **13**, 4436–4442 (2019).

18. May, A. F., Bridges, C. A. & McGuire, M. A. Physical properties and thermal stability of $Fe_{5-x}GeTe_2$ single crystals. *Phys. Rev. Mater.* **3**, 104401 (2019).
19. Zhang, H. et al. Itinerant ferromagnetism in van der Waals $Fe_{5-x}GeTe_2$ crystals above room temperature. *Phys. Rev. B* **102**, 064417 (2020).
20. Deng, Y. Z. et al. Layer-Number-Dependent Magnetism and Anomalous Hall Effect in van der Waals Ferromagnet $Fe_5GeTe_2$. *Nano Lett.* **22**, 9839–9846 (2022).
21. Zhang, G. et al. Above-room-temperature strong intrinsic ferromagnetism in 2D van der Waals $Fe_3GaTe_2$ with large perpendicular magnetic anisotropy. *Nat. Commun.* **13**, 5067 (2022).
22. Wang, C. et al. Sign-tunable exchange bias effect in proton-intercalated $Fe_3GaTe_2$ nanoflakes. *Phys. Rev. B* **107**, L140409 (2023).
23. Guo, J.-j et al. Temperature and thickness dependent magnetization reversal in 2D layered ferromagnetic material $Fe_3GeTe_2$. *J. Magn. Magn. Mater.* **527**, 167719 (2021).
24. Zhuo, W. Z. et al. Thickness-dependent electronic structure in layered $ZrTe_5$ down to the two-dimensional limit. *Phys. Rev. B* **106**, 085428 (2022).
25. Cui, J. H. et al. Layer-Dependent Magnetic Structure and Anomalous Hall Effect in the Magnetic Topological Insulator $MnBi_4Te_7$. *Nano Lett.* **23**, 1652–1658 (2023).
26. Lee, P. A. & Ramakrishnan, T. V. Disordered electronic systems. *Rev. Mod. Phys.* **57**, 287–337 (1985).
27. Gornyi, I. V., Mirlin, A. D. & Polyakov, D. G. Interacting Electrons in Disordered Wires: Anderson Localization and Low-*T* Transport. *Phys. Rev. Lett.* **95**, 206603 (2005).
28. Anderson, P. W. Absence of Diffusion in Certain Random Lattices. *Phys. Rev.* **109**, 1492–1505 (1958).
29. Liu, S. et al. Wafer-scale two-dimensional ferromagnetic $Fe_3GeTe_2$ thin films grown by molecular beam epitaxy. *npj 2D Mater. Appl*. **1**, 30 (2017).
30. Roemer, R., Liu, C. & Zou, K. Robust ferromagnetism in wafer-scale monolayer and multilayer $Fe_3GeTe_2$. *npj 2D Mater. Appl*. **4**, 33 (2020).
31. Nagaosa, N. et al. Anomalous Hall effect. *Rev. Mod. Phys.* **82**, 1539–1592 (2010).
32. Ohno, H. et al. Magnetotransport properties of p-type (In,Mn)As diluted magnetic III-V semiconductors. *Phys. Rev. Lett.* **68**, 2664–2667 (1992).
33. Zhuo, W. et al. Manipulating Ferromagnetism in Few-Layered $Cr_2Ge_2Te_6$. *Adv. Mater.* **33**, 2008586 (2021).
34. Ohno, H. et al. Electric-field control of ferromagnetism. *Nature* **408**, 944–946 (2000).
35. Zhang, R. & Willis, R. F. Thickness-Dependent Curie Temperatures of Ultrathin Magnetic Films: Effect of the Range of Spin-Spin Interactions. *Phys. Rev. Lett.* **86**, 2665–2668 (2001).
36. Tian, Y., Ye, L. & Jin, X. Proper Scaling of the Anomalous Hall Effect. *Phys. Rev. Lett.* **103**, 087206 (2009).
37. Zhang, G. et al. Room-temperature Highly-Tunable Coercivity and Highly-Efficient Multi-States Magnetization Switching by Small Current in Single 2D Ferromagnet $Fe_3GaTe_2$. *ACS*. *Mater. Lett.* **6**, 482–488 (2024).
38. Meng, K. et al. Gate-tunable Berry curvature in van der Waals itinerant ferromagnetic $Cr_7Te_8$. *InfoMat*, e12524 (2024).
39. Wu, L. et al. Anomalous Hall effect in localization regime. *Phys. Rev. B* **93**, 214418 (2016).
40. Wang, X. et al. Pressure-induced modification of the anomalous Hall effect in layered $Fe_3GeTe_2$. *Phys. Rev. B* **100**, 014407 (2019).

## Acknowledgements
This work was supported by the National Key Research and Development Program of the Ministry of Science and Technology of China (Grants No. 2022YFA1602601), the National Natural Science Foundation of China (Grants No. 11888101 and 12004365), the Innovation Program for Quantum Science and Technology (Grant No. 2021ZD0302802), and the Anhui Initiative in Quantum Information Technologies (Grant No. AHY160000).

## Author contributions
X.H.C. conceived and coordinated the project. M.J.W. developed device fabrication techniques and performed measurements with assistance from B.L., K.J.Z., Y.Z.D. M.J.W., B.L., T.W., Z.J.X. and X.H.C. analyzed and discussed the data. M.J.W., B.L., Z.J.X. and X.H.C. wrote the manuscript. All authors discussed the results and commented on the manuscript.

## Competing interests
The authors declare no competing interests.

## Additional information
**Supplementary information** The online version contains supplementary material available at https://doi.org/10.1038/s41699-024-00460-1.

**Correspondence** and requests for materials should be addressed to Bin Lei or Xianhui Chen.